3 Experimental

Many physical analytical techniques are currently in use to get information on the morphological, structural and electronic properties of materials. Most methods are based on the principle of irradiating the sample with particles or photons, and detecting either particles or photons resulting from the interaction. Diffraction effects may occur, time and spatial resolution can be achieved, and different energy ranges can be used. To each combination of probes and effects corresponds a specific technique. The sample can be in ambient conditions only in the case of photons with a wavelength longer than 200 nm. Otherwise sample, source and/or detector have to be placed in vacuum or ultra high vacuum (UHV, a pressure below 10^{-9} mbar). Such conditions are favorable also to handle substances which would react with atmospheric water or oxygen.

Diffraction techniques such as x-ray diffraction (XRD), extended x-ray absorption (EXAFS), low energy electron diffraction (LEED), high resolution transmission electron microscopy (HRTEM), scanning microscopies (atomic force, AFM and electron tunneling, STM) provide information either on the short or long range structure. For measuring electronic properties optical absorption spectroscopy, impedance, Hall effect, magnetic susceptibility, electron spin resonance (ESR), nuclear magnetic resonance (NMR), etc. are used. The electronic structure can be postulated and used to fit XANES (x-ray absorption near-edge) spectra. All these techniques reflect some aspects of the electronic properties of the material in a more or less indirect way. A direct measurement is possible with electron scanning tunneling spectroscopy (STS), but only limited to the Fermi level region. The analytical tool used in this work to characterize all prepared materials is Photoelectron Spectroscopy (PES), the only technique which provides a direct and exhaustive measurement of the electronic structure of the investigated material. But as it is basically a surface sensitive technique, care must be taken that indeed bulk properties are probed, which needs a specific preparation procedure of the samples.

In this chapter the fundaments of PES, the operation in UHV and experimental details on sample preparation will be given. An introduction to two ex-situ microscopies used for the thin film characterization, and the special sample preparations that were necessary for these measurements will close the chapter.

3.1 Photoelectron spectroscopy

Literature on a well-established technique such as photoelectron spectroscopy is of course abundant. Comprehensive overviews can be found e.g. in refs. [130-132]. In this section only elements of relevance to this dissertation will be treated.

3.1.1 Basics

The principle of photoemission was first explained by Einstein in 1905, in the frame of his theory on light quanta [133]. Photons can interact with electrons and transfer their energy $h\nu$ exciting the electron from an occupied to an higher unoccupied state. If the excitation energy $h\nu$ is larger than the binding energy W of the electrons to a system, the electron will escape the system with a kinetic energy E_{kin}, according to the energy conservation principle:

$$E_{kin} = h\nu - W \qquad \textit{(Eq. 3.1).}$$

In the 60s K. Siegbahn's research group developed a technique based on this effect where a resolution <1 eV could be attained, so that it was possible to distinguish among different chemical states for a given element. For this reason the technique was called Electron Spectroscopy for Chemical Analysis (ESCA), but today it is better known as x-ray photoelectron spectroscopy (XPS). For this achievements Siegbahn was awarded the Nobel Prize for Physics in 1981. Since the 70s the technique has been integrated into commercial surface analysis equipments.

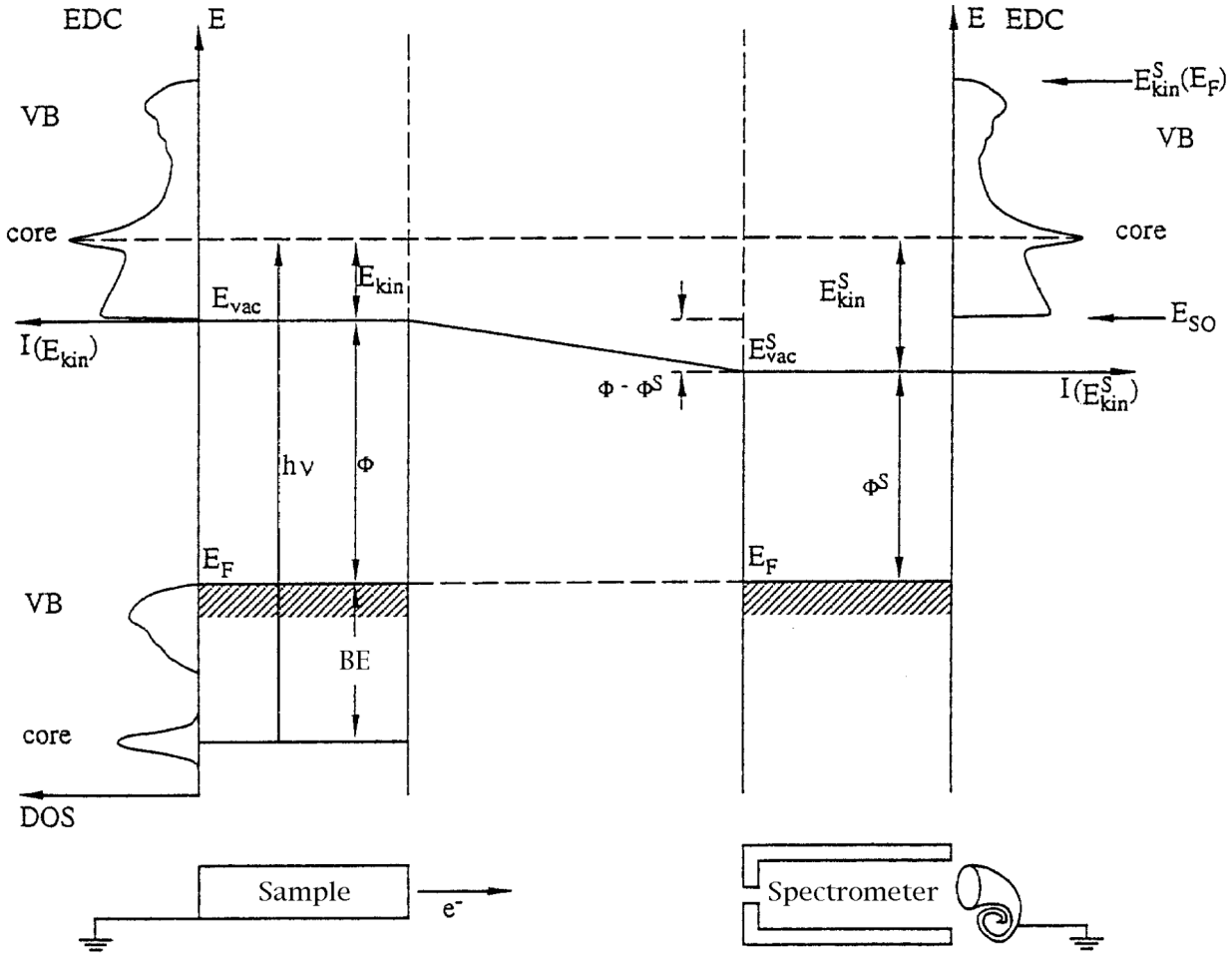

Fig. 3.1 Scheme of the photoemission process as measured by a spectrometer (from ref. [134])

A solid sample is irradiated with x-rays in vacuum, so that emitted electrons can reach an analyzer where they are counted in a selected energy range. It is then possible to obtain the energy distribution curve (EDC), a plot of the number of electrons collected as a function of their kinetic energy. The number of collected electrons corresponds in a first approximation to the density of (occupied) electronic states (DOS). For convention W is split into two terms, the binding energy BE and the work function Φ, so that the energy distance of the emitting electronic state from the sample Fermi level (E_F) is BE. BE is the typical value used to represent the energy scale. Eq. 3.1 can then be written as

$$E_{kin} = h\nu - (BE + \Phi) \qquad \textit{(Eq. 3.2).}$$

Sample and spectrometer are kept in electrical contact, so that a common Fermi level exists, but the analyzer work function Φ^S is in general different from that of the sample. The kinetic energy E_{kin}^S measured by the analyzer differs from E_{kin} because of the acceleration (or retardation) due to the electrical field between sample and analyzer (Fig. 3.1). The measured kinetic energy is thus

$$E_{kin}^S = h\nu - (BE + \Phi^S) \qquad \textit{(Eq. 3.3).}$$

If a metallic sample is used, E_{kin}^S measured for the Fermi edge (BE=0) can be readily identified at the largest kinetic energy where signal intensity is detected. Given the photon energy, Φ^S is obtained and then also the BE scale:

$$E_{kin}^S(E_F) - E_{kin}^S = BE \qquad \textit{(Eq. 3.4).}$$

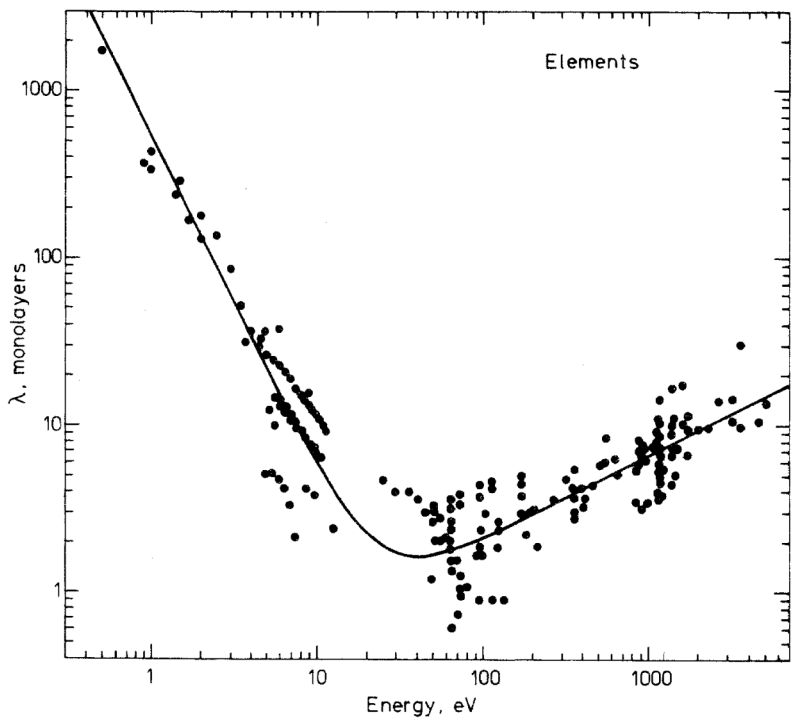

Fig. 3.2 Mean free path of photoelectrons emitted from different elements and lines (from ref. [135])

Photons of energies up to 1200 eV can penetrate a solid a few μm. But the free mean path λ_e of electrons in a solid depends on their kinetic energy, and is nearly independent of the material, so that a universal curve can be traced as reported in Fig. 3.2. A minimum is found for E_{kin} = 50-70 eV with a distance of 2 atomic monolayers, corresponding to about 5 Å. For larger energies λ_e increases proportionally to $E_{kin}^{1/2}$, reaching a value of 10 monolayers for 2000 eV. Since just a few top monolayers can be detected, photoelectron spectroscopy is a typical surface science technique.

3.1.2 The photon sources

PES is based on photonic excitation from a monochromatic source. Three adequate light sources are known, which originate each a specific spectroscopy. Typically used soft X-ray sources emit the lines Mg and Al Kα. Their highly energetic radiation is able to ionize characteristic bulk energy levels. For this reason XPS is used as chemical analysis tool. With a monochromator it is possible to achieve a width, and thus a signal energy resolution better than 100 meV, but at the expenses of the light intensity. For this work only the Mg Kα X-ray radiation has been used without any monochromator.

The UV light emitted from noble gas discharge lamps can ionize electrons from valence bands and shallow core-levels. Typical used emission lines are the He I α and He II α lines; their width is particularly small. Compared to X-rays, UV light has a much larger cross section for valence band states [136]. Also the analyzer sensitivity is typically higher at lower kinetic energy. For these reasons UPS allows to obtain well resolved valence band spectra.

In a synchrotron electron packets run along a circular ring, and because of their acceleration they emit electromagnetic radiation tangential to their orbit. The light has a broad spectral distribution, and the energy can range from far-infrared to the x-rays. In the orbit plane it is linearly polarized, elsewhere elliptically. The synchrotron light used in this work originated at the Berliner Synchrotron facility (BESSY I), at the beam line TGM-7. The light beam has an area of less than 1 mm^2, and with a monochromator the required light energy can be selected. The line width is typically much smaller than with XPS, and depends on the monochromator specifications. With synchrotron induced X-ray PS (SXPS) it is possible to investigate states at variable excitation energy and/or constant kinetic energy. The technique is particularly important for the study of adsorbates and surface states, where it is important to keep the information depth of the signal minimal and constant. Additionally, states that have a weak XPS cross section may be easily measured at hν=80 eV, as in the case of Li 1s. Depending on the synchrotron and the monochromator, radiations in the range 5-5000 eV can be obtained.

Emission	Photon energy (eV)	Line width (meV)	Flux (photons/s)
Mg Kα	1253.6	680	$1 \cdot 10^{12}$
He Iα	21.22	3	$1 \cdot 10^{12}$
He IIα	40.82	17	$2 \cdot 10^{11}$
BESSY I (TGM 7)	10-120	300	$\geq 10^{13}$

Tab. 3.1 Photon energy and line widths of the excitation radiations used in this work

3.1.3 The electron analyzer

Photoelectrons are emitted in various directions, with a distribution, which depends also on momentum distribution of their initial state. This can play a role for the shape of the measured valence bands of single crystalline materials. To maximize both the angle integration and the spatial resolution to which spectra refer, an optical system based on magnetic lenses focuses on the sample surface. Most XP spectrometers are based on a concentric hemispherical analyzer. It consists of two hemispherical metal surfaces and between them a voltage ΔV is applied with the outer sphere at a more negative potential (Fig. 3.3). A slit is on one side and a channeltron or a multichannel electron detector is at the other. Electrons coming to the entrance slit are deflected and reach the detector only if their energy corresponds to the pass energy E, which is a function of ΔV. The sample is grounded, and in our operation mode during a scan the spectrometer potential is swept so that electrons of all energies can be retarded to the constant pass energy value at the entrance slit. With this analyzer geometry the energy resolution ΔE is such that ΔE/E is proportional to S/R, where S is the entrance slit width, and R the mean of the two hemisphere radii. Geometry is typically chosen to have ΔE/E=1/100.

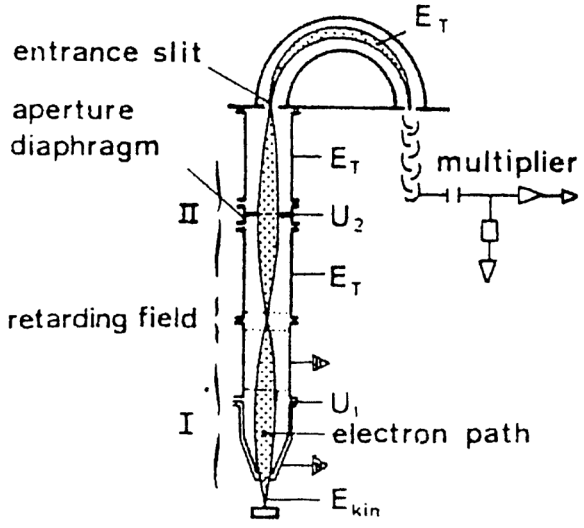

Fig. 3.3 A concentric hemispherical analyzer provided with magnetic lenses. From ref. [137]

3.1.4 Spectra and interpretation

In this work the electron binding energies will be given as difference from the Fermi energy. According to this convention a lower kinetic energy corresponds to a higher BE. The peak corresponding to the core levels are indicated with the main quantum number and the orbital angular momentum (s, p, d, f) of the hole left in the final state. With adequate resolution the structure of the electronic states can be recognized. The hole spin-orbital coupling is visible as a doublet in the splitting of each level having an orbital quantum number $l>0$. The two components correspond to the two possible total angular momenta *j*, which are therefore indicated as $l-1/2$ and $l+1/2$; their intensity is proportional to the degeneracy of these states $(2j+1)$. In general when the BE for a doublet is given, this identifies the position of the more intense component ($l+1/2$). Each element has a characteristic disposition of electronic states that can be easily recognized in a spectrum which extends between 1100 and 0 eV. An example of overview spectrum is reported in Fig. 3.4). Only H and He cannot be detected. All other elements can be detected down to a sensitivity of the order of 0.1 atom percent. The peak position can vary within several eV in dependence of the element's chemical environment, which can be used for chemical identification. In general it can be stated if the electron density at one atom is larger the BE of the corresponding core levels is lower. As a consequence the largest influence on this chemical shift is the oxidation state: electrons from a more reduced (oxidized) atom have a lower (higher) binding energy. Differences can reach some eV, and characteristic binding energies for many compounds are given in several literature surveys [138, 139].

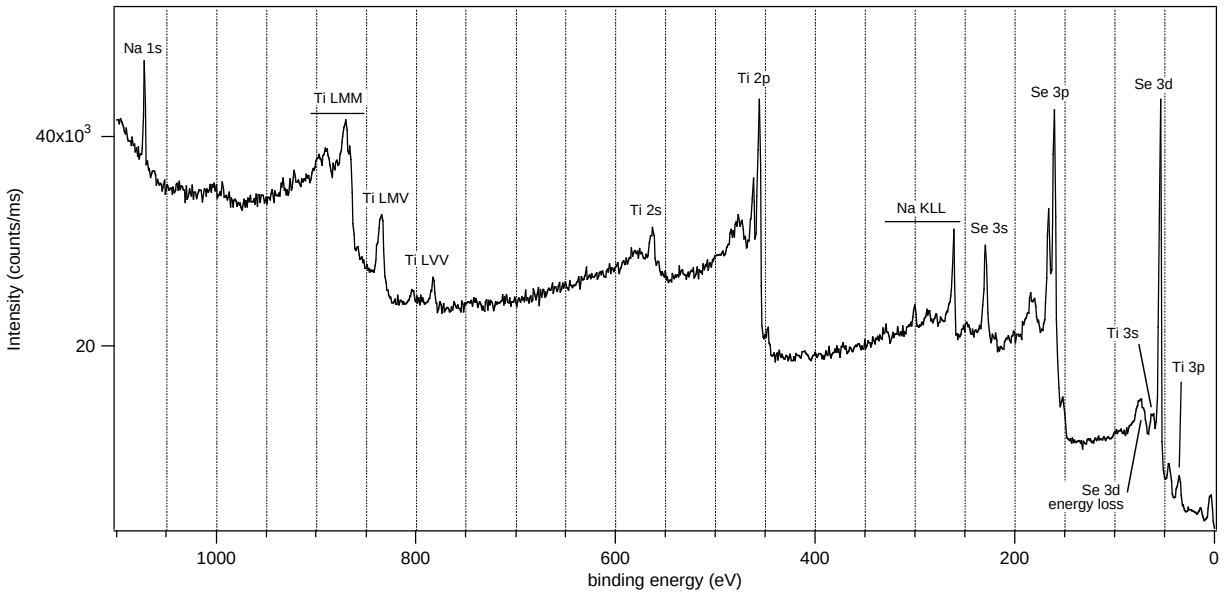

Fig. 3.4 Overview XPS spectrum taken on a Na-intercalated $TiSe_2$ cleaved crystal

The peak positions may also change due to sample charging after the ionizing process. For conducting specimens this is avoided because emitted electrons are replaced with an electron flow

from the spectrometer in electric contact with the sample. The conductivity is much smaller for insulators, and a static positive charge builds up, increasing the observed BEs by up to several eV. It will be then necessary to refer values to the position of an element of known BE. For polymers, as an example, usually the C 1s signal is taken as an internal reference.

The secondary emission background

The electrons leaving the material without further interactions after their excitations are called primary electrons. But during the escape process electrons may also loose part of their energy due to inelastic scattering in the sample, and these are called secondary electrons. Being a random process the secondary emission shows no specific energy. The EDC results from the overlapping of both primary and secondary emission. For statistic reasons the intensity of the secondary emission for a given energy is roughly proportional to the total emission at higher kinetic energies. Starting from the Fermi level, towards lower kinetic energies the EDC is typically increasing because of the secondary emission background. At the point corresponding to the zero (sample) E_{kin} the EDC drops suddenly, since electrons with lower energy cannot be emitted (see for example Fig. 3.5). This point is called secondary emission onset, and from its binding energy BE^{so}, given the spectra excitation based on Eq. 3.2 the sample work function Φ can be calculated:

$$\Phi = h\nu - BE^{so} \qquad \textit{(Eq. 3.5).}$$

The overall shape of the secondary emission can give information on the sample morphology. In XPS a flat secondary emission is generally considered as a sign of sample homogeneity. But normally quantitative analytic information is obtained from the primary emission. It is then necessary to remove the background properly. This is done by subtracting a function fitted to the peak tails. The choice of the background function influences both the peak shape and intensity, and is not straightforward for many compounds. As an example metals are affected by shake-up events, when conduction electrons are excited simultaneously with photoelectrons, which then appear at lower energy. This causes a so-called intrinsic background which affects the peak symmetry and may extend for hundreds eV.

For practical purposes simplified functions are used. In XPS spectra the Shirley method was used, which assumes the background as originated only from inelastic scattering of electrons having higher kinetic energy. The integrated EDC [140, 141] is a step-like function. For SXP spectra instead a 2nd or 3rd grade polynomial is more appropriated. The intensity and the shape of the background-removed peaks can then be evaluated. All mathematical treatments of PS data for quantitative analysis were executed with procedures written for the Wavemetrics IGOR application [142].

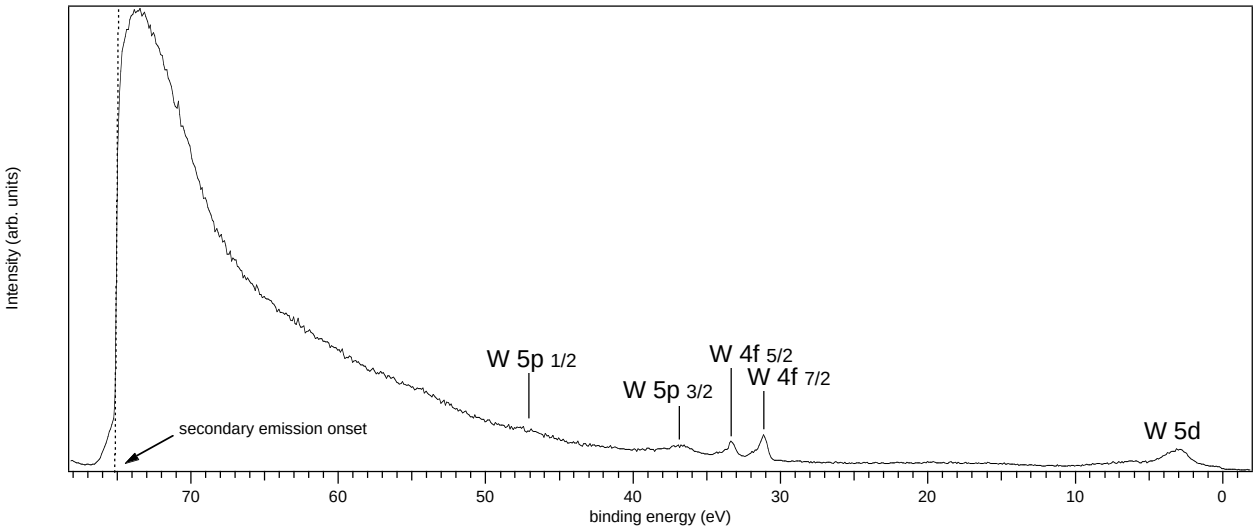

Fig. 3.5 Overview SXP spectrum taken at BESSY/TGM 7 on a deposited metallic W film with an excitation energy hν = 80 eV

The peak intensity

The current I_A^X of photoelectrons leaving the sample with kinetic energy *E* from the level X depends in a rather complex way from the amount of the emitting element A:

$$I_A^X = \sigma_A^X D(E) \int_{\gamma=0}^{\pi} \int_{\phi=0}^{2\pi} L_A^X(\gamma) \int_{y=-\infty}^{\infty} \int_{x=-\infty}^{\infty} J(x,y) T(x,y,\gamma,\phi,E_A) \int_{z=0}^{\infty} N_A(x,y,z) \exp\left[\frac{-z}{\lambda_M(E_A)\cos\theta}\right] dz dx dy d\phi d\gamma$$

(Eq. 3.6),

where *E* is the spectrometer pass energy, E_A the photoelectron kinetic energy, and the other independent variables are defined as in Fig. 3.6; σ_A^X is the ionization cross-section for the observed level X, *D* the detector efficiency, L_A^X is the angular dependency of the emission, *J* the x-ray photon flux at the point (x,y) of the sample, *T* the spectrometer transmission function, N_A the atom density, λ_M the electrons free mean path (which depends also on the material matrix). I_A^X corresponds to the peak height above the background for a given E_A; by comparing peaks the integrated peak area is a reliable value. Given the typical inaccuracy in the background removal, which affects the measured intensity, simplifications to Eq. 3.6 are convenient for practical analytical purposes.

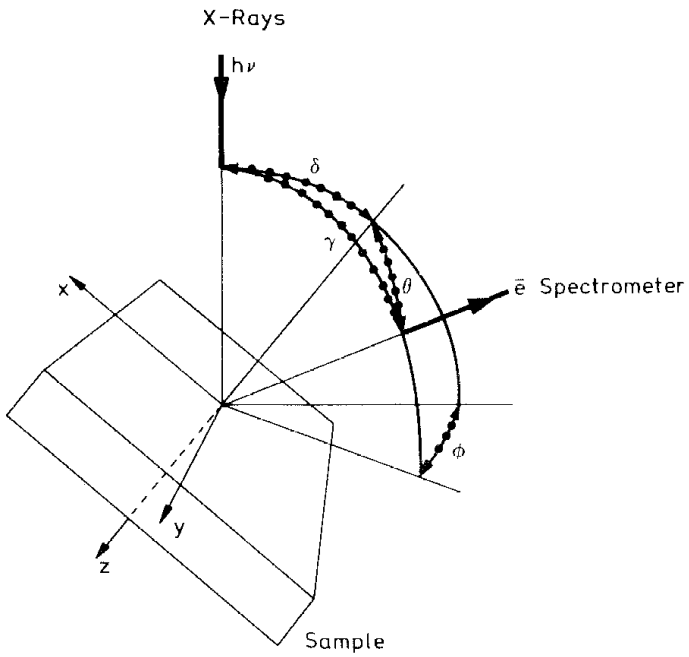

Fig. 3.6 Geometry of the XPS measurement configuration

In general we are interested to know only the relative molar fractions, assuming a homogeneous material over several times λ. If we assume only contributions from the given γ, ϕ geometry and that *J* and *T* are constant all over the sample area *A* from which photoelectrons can be detected, then Eq. 3.6 reduces to

$$I_A^X = \sigma_A^X D(E) L_A^X(\gamma) JT(E_A) N_A \lambda_M(E_A) A \qquad \textit{(Eq. 3.7).}$$

The cross section σ reflects the probability that incident photons cause the ionization of a specific core-level; it depends on the photon energy, and the values are known from theoretical calculations [136]. The detector sensitivity *D* does not play a role in ratios, if measurements are in constant pass energy *E* modus. L_A^X depends on the spectrometer geometry. Its calculated value depends on the tabulated values of β_A^X, given by [143] as

$$L_A^X(\gamma) = 1 + \frac{1}{2}\beta_A^X\left(\frac{3}{2}sin^2\gamma - 1\right) \qquad \textit{(Eq. 3.8).}$$

The transmission function is instrument-specific.

The most rigorous method for quantitative analysis is to record reference data using the same instrument under the same conditions avoiding any surface contamination. Reference data can be measured from the pure elements (below indicated with the index ∞). It can be easily shown that assuming λ independent from the material matrix

$$\frac{N_A}{N_B} = \frac{N_A^\infty}{N_B^\infty}\frac{I_B^\infty}{I_A^\infty}\frac{I_A}{I_B} \qquad \textit{(Eq. 3.9).}$$

N^{∞} represents the number of element atoms per unit volume, so that in the above expression only the intensities for the pure elements must be measured. Alternatively a compound of known stoichiometry can be used as a reference. An expression analogous to Eq. 3.9 can be used, where the reference concentration ratio is the stoichiometric proportion. In spite of the approximations due to surface contamination, possible different surface roughness, and matrix-dependent λ, the accuracy of this method can be estimated to be 10% [144].

A practically easier method is to use published data sets, which are usually recorded under different conditions. The reported values depend on the effects of angular anisotropy, as well as analyzer and detector characteristics, which may be affected by the used calibration. From Eq. 3.7 an area sensitivity factor $S_A^X = \sigma_A^X L_A^X(\gamma) AT(E_A) D(E) \lambda(E_A)$ can be defined, such that stoichiometries can be easily given by

$$\frac{N_A}{N_B} = \frac{S_A}{S_B}\frac{I_A}{I_B} \qquad \textit{(Eq. 3.10).}$$

The *S* values found on tables are typically referred to the F 1s signal, so that S_F^{1s}=1. The validity of this formula relies on the assumption that if not *S*, the ratio $S_A/S_B \propto \lambda_A/\lambda_B$ is only slightly matrix dependent. The angular term *L* has no significant influence compared to other factors. The *ATD* product depends strongly on the spectrometer, and tables of area sensitivity factors can give largely scattered values for the same XPS core level. The detailed knowledge of the characteristics of reference and used spectrometers and materials would also allow an accuracy in the order of 10% [145].

Instead of using published area sensitivity factors, which only in ideal cases are reliable within 10%, relative stoichiometries given in this work were estimated from the core level intensity ratios corrected by theoretical cross sections for the used photon energy and by the spectrometer transmission function. With compounds of known stoichiometry these factors gave errors often below 10%.

The peak shape

The measured signal deviates from the ideal line because of a broadening caused by the hole state life time and by the instrumental energy resolution. The two effects on the signal shape are represented by a Lorenzian and a Gaussian function respectively, which are convoluted in a Voigt profile. For practical purposes, a least square fit of the experimental data with the convoluted function is too time demanding, and the approximation below is preferred [146]:

$$I(E) = I_0 \Big/ \left(\left(1 + \frac{4\Delta^2 M}{\Gamma^2} \right) \exp \frac{4 \cdot \Delta^2 (1 - M) \ln 2}{\Gamma^2} \right) \qquad \textit{(Eq. 3.11),}$$

$$\text{where}\,\Delta = \frac{E - E_0}{1 - \alpha \dfrac{(E - E_0)}{\Gamma}}.$$

The five parameter to fit for a single peak are: I_0 intensity, E_0 binding energy, Γ is the peak full width at half maximum (FWHM), α asymmetry factor (it can account for effects like inelastic electron-phonon scattering as typical in metals), M the Gauss-Lorenz fraction (M=0 pure Gauss, M=1 pure Lorenz). To reduce the degree of freedom during parameter fitting and obtain acceptable values constraints are applied, or theoretical or known (from literature or reference measurements) values are taken. For a doublet the same Γ, α and M are taken, while the intensity ratio must be a value close to the theoretical $l/(l+1)$.

Auger emission

The filling of an electronic level after ionization implies emission of x-ray photons. The detection of these photons originates the EDX spectroscopy technique. As a concurrent process the hole can be filled by an electron from a level above, and the remaining unpaired electron is emitted with a characteristic kinetic energy. This effect was discovered by Pierre Auger and the corresponding emission spectroscopy (AES) was developed, which relies on electronic irradiation. Auger signals are also detected in XPS. Auger electrons can be easily recognized by changing the excitation source: their kinetic energy is constant, and thus the BE of Auger peaks would change their positions. Auger peaks appear as groups and are labeled after the electronic shell involved in their emission, according to the spectroscopic K, L, M, N, …,V nomenclature.

Further aspects

The description given so far can explain the main features of photoemission spectra. However the photoemission process is rather complex, and a number of aspects requires a more detailed knowledge of the involved mechanism. The quantum mechanic many-body effect of photoemission is often simplified in a three step model, where electrons are 1) excited to a higher level, 2) transported through the solid, 3) escape from the surface. Steps 2 and 3 have already been anticipated, in their effects on the secondary emission (inelastic scattering) and work function (potential barrier at the surface). The first step leads to the most significant structures in the spectra. It depends on the transition probability, which results from the dipole matrix element and the product of the joint density of initial and final state. The spectra are not just a picture of the material at its fundamental state. For small kinetic energies (10 eV or less) the structure of the final state density can play an important role; with higher energies the behavior of free electrons is assumed, with the corresponding constant density of states. Only in this case the EDC can be assumed as a near approximation of the DOS in the initial state.

In metallic samples besides shake-up events energy losses may be due to plasmon excitations. Plasmon-loss structures appear as broad peaks shifted up to 20 eV to larger BE values from the originating core level line. As an example they are clearly visible in Fig. 3.4 at the left side of the Ti 2s, Ti 2p, Se 3p and Se 3d peaks.

3.2 UHV equipment and spectrometer systems

Due to the requirement that electrons must travel from the sample to the analyzer a vacuum of at least 10^{-6} mbar is required. But due to the technique's surface sensitivity any kind of adsorbates chemically or physically interacting with the sample alter significantly the spectra. With a partial pressure of 10^{-10} mbar one monolayer of a species with unity sticking probability would deposit in 3 hours. In practical cases a total pressure of 10^{-10} mbar generally prevents from contamination within a time much longer than required for the measurements. These vacuum levels can be achieved with standard UHV equipment based on turbo molecular pumps connected to rotary vane or membrane rough pumps typically able to reach a pre-vacuum of $4 \cdot 10^{-2}$ mbar. In absence of leaks after venting, pressures of the order of 10^{-10} mbar are promptly reached only by baking the system for at least 8 h at 130-180°C, depending on the chamber size. This process speeds up the desorption of atmospheric adsorbates (especially water) from the chamber walls. Rest gas molecules can also be temporarily captured by cooling traps, or permanently by titanium sublimation pumps.

During this work three spectrometer systems have been used for photoemission measurements. Cl_2 adsorption and all Li deposition experiments were carried out at BESSY I TGM 7.

All laboratory measurements were done at the Hahn-Meitner Institute Berlin GmbH, using either a VG ESCALab MkII or a Leybold EA11 MCD analyzer, both equipped with x-ray and UV He lamps. The pass energies used are reported in Tab. 3.2. The electron binding energies were calibrated setting the position of Au 4f7/2 at 84.0 eV, for Cu 2p3/2 at 932.7 and the Au's Fermi edge at 0 eV.

	XPS overview	Ti 2p Ta 4f S 2p Se 3d	Na 1s Na KLL	O 1s C 1s Cl 2p	XPS valence band	He I	He II
EA11	126	25.2	25.2	50.4	50.4	6.3	12.6
MK II	100	20	20	50	50	5	20

Tab. 3.2 Typical pass energies values (in eV) used in this work

3.2.1 The ESCALab Mk II

This equipment consists of an analysis chamber with a base pressure of $1 \cdot 10^{-10}$ mbar, a preparation chamber equipped with LEED optics, Ar^+-gun and alkali dispensers, and a synthesis chamber for thin film preparation.

The spherical analyzer of this spectrometer has a transmission function $T \propto 1/\sqrt{E_{kin}}$ and, assuming $\lambda \propto E^{0.5}$ from Eq. 3.12 for the relative elemental concentration the expression

$$\frac{N_A}{N_B} = \frac{\sigma_A^X}{\sigma_B^Y} \frac{I_A}{I_B} \qquad \textit{(Eq. 3.12)}$$

can be derived, therefore taking as sensitivity factors just the theoretical cross sections for the given line at the experimentally used excitation energy.

All experiments of Na intercalation in single crystals and the first attempts of thin film synthesis were carried out with this system.

3.2.2 The integrated system

Thin film preparation and analysis were performed at the so-called “Integrated System”. It contains a cluster of several preparation chambers connected to surface analysis equipment via transfer chambers at pressures below 10^{-9} mbar. Thus any form of air contamination between the synthesis and the measurement steps is excluded. The spectrometer chamber was also equipped with an ion gun, a SIMS mass spectrometer, and a LEED optics, as well as a UHV-STM chamber. The pressure was in the order of 10^{-10} mbar during measurements. For the Leybold EA11 MCD analyzer the acceptance angle is 30°, and with constant pass energy the transmission function is $T \propto E^{-0.7}$, therefore the relative concentrations are calculated, in analogy with Eq. 3.12, as

$$\frac{N_A}{N_B} = \frac{\sigma_A^X}{\sigma_B^Y} \left(\frac{E^X}{E^Y} \right)^{0.2} \frac{I_A}{I_B} \qquad \textit{(Eq. 3.13).}$$

The measure of the Na concentration was of particular importance for the present work. The relation (Eq. 3.13) was verified measuring the intensities of a Na_2SO_4 salt. The experimental value was Na/S=1.87, i.e. within a deviation below 10%.

In contrast to the other systems a specific transfer system is used, based on carriers of the Leybold company. These carriers include the whole heating-thermocouple block, which allows to control the temperature in the preparation as well as in the analysis chambers. The heating consisted of a 0.3 mm thick and ~60 cm long Mo wire inserted into ceramic tubes inside a stainless steel block. The sample mounted on a steel plate was kept in thermal contact to it by two metallic clips. A Ni/Cr thermocouple was screwed to the same block. The disadvantage of this system is a much

larger surface to degas when introducing a new sample into vacuum, but more sophisticated conceptions for the sample treatment are possible, as it will shown later by the experimental results.

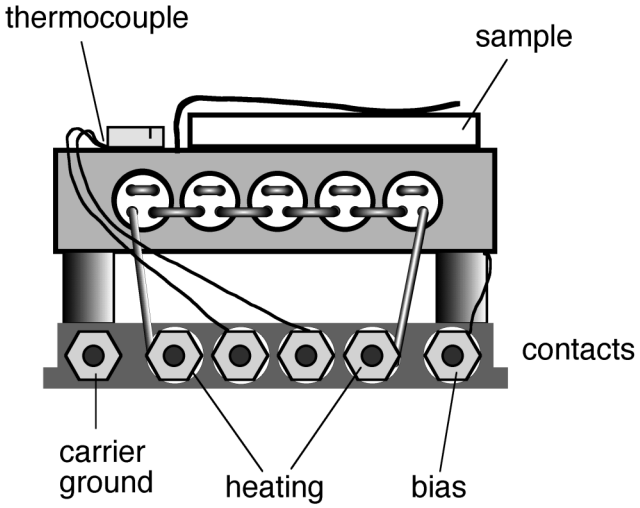

Fig. 3.7 The Leybold sample carrier as mounted for measurement on metallic samples

3.2.3 BESSY

An angle resolving VG ADES 500 spectrometer with an acceptance angle of 2° coupled to the BESSY I TGM 7 beam line was used with a pass energy of 15 eV.

The basal pressure in the analysis chamber was $3 \cdot 10^{-11}$ mbar. It was possible to heat or cool the manipulator within the temperature range 100-400 K. In the main preparation chamber crystals were cleaved and alkali were deposited. For Cl_2 adsorption at low temperatures a chamber was mounted on top of the analysis chamber; during these experiments alkali were evaporated directly in the analyzer chamber.

As already pointed out in §3.1.2 the TGM 7 photon energy range is specifically suited for adsorption experiments and for the Li 1s signal. Other well detectable core levels were Na 2p, Ta 4f, and Se 3d. Ti, S, C, O, Cl have no core-level lines with large cross sections for photon energies of 10-120 eV. However, in the case of Cl valence band states are well visible. With the photon energy of 80 eV the kinetic energies of all core levels range between 30 and 70 eV, and the analyzer transmission function, as well as the free mean path λ can be considered constant.

Due to collisions of the ring electrons with residual gas molecules (pressure inside the ring was about 10^{-10} mbar) the photon intensity was decreasing exponentially with time ($t_{1/2} \approx 4$ h). The emission intensity was also decreasing proportionally. To compare different lines and their intensity all spectra are normalized by the photoemission current measured by a detector placed in front of a mirror in the monochromator. The intensities will be given in arbitrary units proportional to the signal measured at constant photon flux.

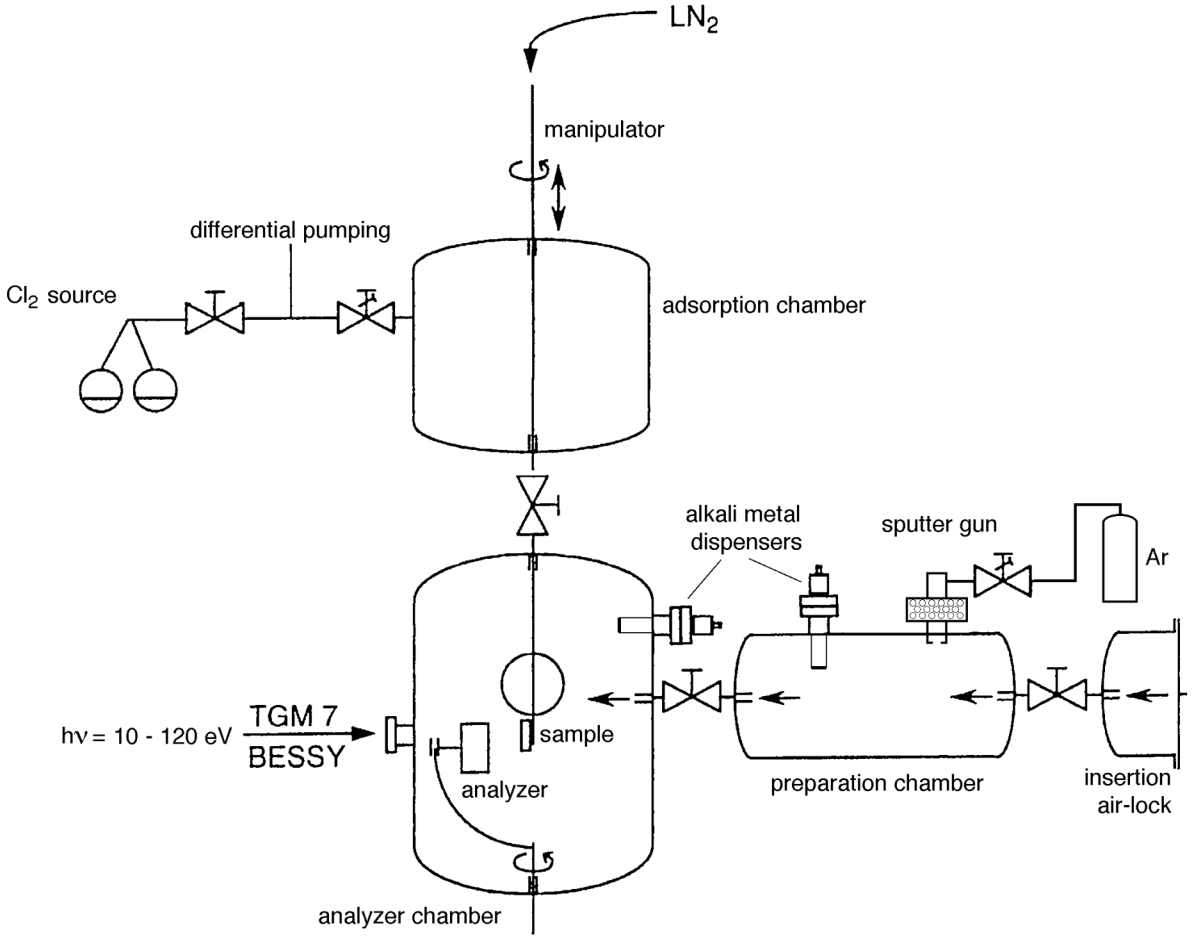

Fig. 3.8 A scheme of the experimental set-up at the BESSY I TGM 7 beam line

3.2.4 Preparation chambers

Depending on the operation, two kind of preparation chambers have been used during this work.

For substrate preparation and alkali deposition a chamber with a base pressure of the order of $5 \cdot 10^{-10}$ mbar was used. In this chamber the crystal surfaces were prepared. TMDC single crystals were attached to the sample holder with Ag epoxy at air, and a Mo foil was attached to the top of the crystal. Lifting off the foil from the surface the crystal could be cleaved to obtain nearly ideal defect-free surfaces.

Thin films of TMDCs were prepared in high vacuum in a small volume spherical deposition chamber (Fig. 3.9) directly from the elements or from other molecular precursors. Two flanges were used for precursor sources, while a smaller hosted a Ti source at a position closer to the transfer rod. The sample carrier could be inserted on a linear transfer motion unit (LTM) opposed to the sources. Thus the sample could be moved from the transfer position to a distance where both precursor fluxes could be considered to cover it homogeneously. In order to increase the precursors local

pressure tiny guide tubes were inserted at the vacuum side of the valves, which kept the evaporating beam focused up to a distance of about 3 cm from the sample. The sample electric heating was provided by a power supply connected to a switch between two digital PID (proportion, integral and derivative) regulators which used as feedback the sample temperature and the total chamber pressure respectively. While the first one was used to program ramps during deposition, the latter was used for degassing samples at constant pressure (and then automatically increasing the temperature). The sample transfer was operated with a magnetically coupled feedthrough to the preparation chamber and subsequently to the analysis chamber. A quadrupole mass spectrometer (Balzers QMA 125) was also connected for a limited period, in order to inspect partial gas composition of the chamber during deposition.

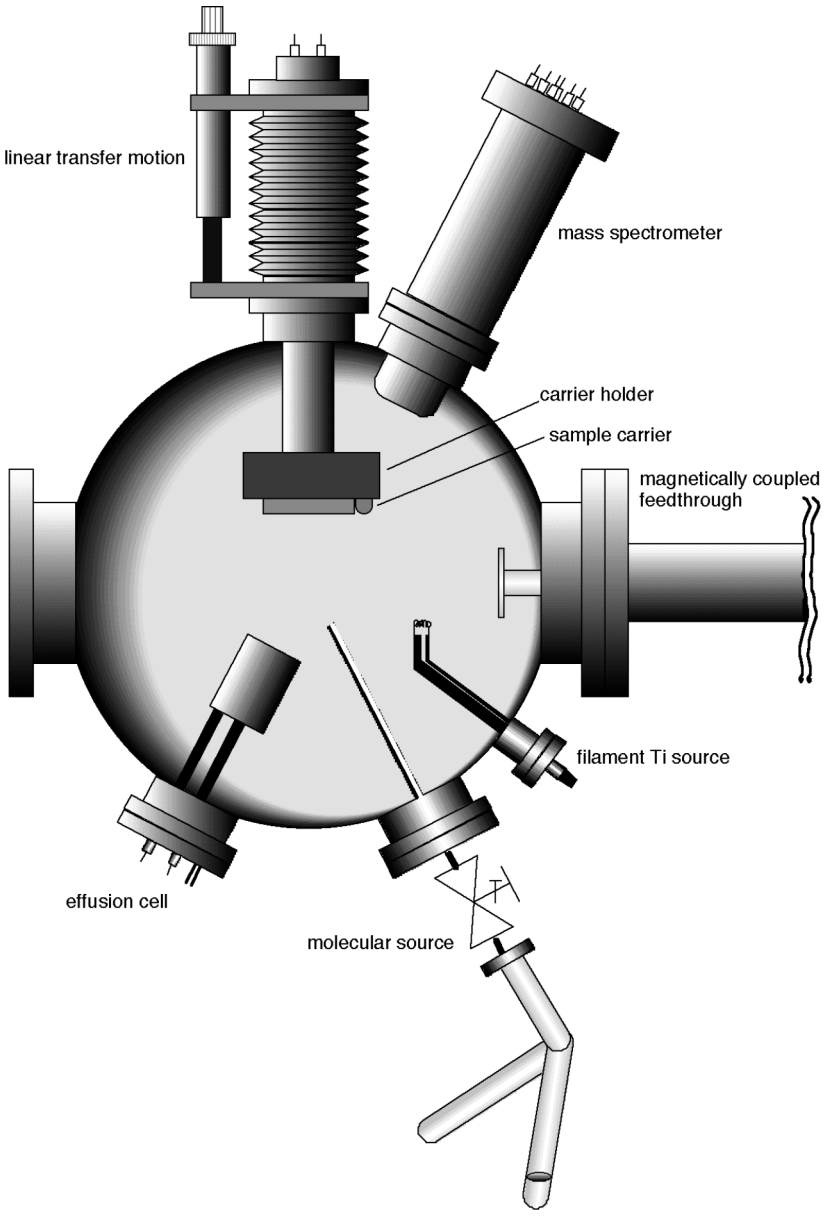

Fig. 3.9 The thin film preparation chamber

3.3 Preparative methods

3.3.1 Samples

Single crystals

TMDC single crystals as provided by Dr Y. Tomm were attached to clean Cu holders with conductive Ag epoxy. On top a 0.1 mm thick Mo foil was glued. After drying for at least 3 h at 80°C, the samples were transferred to the UHV system. Once in the preparation chamber at a maximal pressure of $5 \cdot 10^{-9}$ mbar the crystal could be cleaved exposing typically 5-10 mm sized clean and mirror-like surfaces.

Metal substrates

Metallic foils used for thin film preparation were rasped and cleaned with acetone in a ultrasound bath. After transfer to UHV they were outgased in the preparation chamber, by heating at a constant pressure of $2 \cdot 10^{-7}$ mbar until, typically after half an hour a temperature >400°C was reached. Further cleaning was performed with 5 min Ar^+ sputtering at 5 kV and 2 μA.

3.3.2 Sources

Alkali metals

Alkali metals were evaporated from dispensers produced by SAES Getters SpA. The dispensers are constituted by a mixture of the respective alkali chromate (A_2CrO_4) and an Al alloy (ST101:16% Al/ 84% Zr) enclosed in a nickel boat. By resistively heating at currents larger than 4.5 A temperatures >500°C are reached in vacuum and the alkali is reduced by the alloy. Due to its special shape the boat opens and the alkali are emitted through a narrow slit. For Li, Na, Cs, respectively currents of 8.5 A, 7.0 A and 6.5 A were used, which correspond to temperatures of 900-700°C. The evaluation of the evaporation rate is particularly difficult and dependent on the source's operation time. A measure of the deposition rate with a quartz microbalance is impossible, since at room temperature alkali are known to stick only up to one monolayer on different substrates. Practically the amounts of alkali on the samples are always evaluated from their XPS signal relative to the substrate.

Metallic Ti

The relatively low melting point of Ti allows the use of a filament as source for metallic Ti. A thin filament has to be used, as it is clear from the expression of the power as function of voltage and current, or filament resistivity, length and section:

$$P = V \cdot I = R \cdot I^2 = \rho \frac{l}{S} I^2 \qquad \textit{(Eq. 3.14).}$$

A 0.1 mm thick foil (99.9% Ti) was cut to a 1.5 mm wide and 60 mm long ribbon, and bent to a 1 cm long coil. It was possible to increase the power up to a value at which a closed coating of pure Ti could be obtained after 20 minutes deposition onto a substrate kept at a temperature below 100°C. Although at the fixed distance of about 2 cm the sample temperature could not be kept at RT, Ti was found to easily stick on a wide range of surfaces.

Elemental chalcogen sources

S_2 was obtained as decomposition product of pyrite (FeS_2) crystals heated in an effusion cell crucible to temperatures of 200-320°C. Compared to elemental S crystals as precursor, this source has the advantage of being bakeable inside the vacuum system. In addition a high S_2 yield is obtained instead of less reactive S_x chains. But the evaporation rate at a fixed temperature is not constant.

With the same principle WSe_2 crystal flakes were used for Se. They were rolled into a thin Ta foil where small holes were opened. By resistively heating WSe_2 decomposed inside the foil and Se_2 evaporation could be obtained.

Metal organic molecular sources

The metal organic precursors used for deposition ($TiCl_4$, TBDS, HMDST) are liquids with elevated vapor pressure at RT. In an Ar-filled glove box an amount of about 1 ml was filled into a twin glass tube which was closed with a fine dosing valve and mounted to the UHV system (see Fig. 3.9). Ar and eventual volatile impurities could be evacuated by opening the valve to the vacuum after freezing the liquids at the dry ice temperature (-78°C). For further purification the liquid was distilled to the empty tube at least three times and again frozen and evacuated.

The advantages of these sources are their large capacity and constant rate which can be controlled with good precision by the total pressure measured in the chamber.

Gas sources

For Cl_2 and H_2S gases glass test tubes connected to the UHV chamber through fine dosing valves were used. The doses are expressed in Langmuirs [L], as given by:

$$1\,\mathrm{L} = 10^{-6}\ \mathrm{Torr}\cdot 1\,\mathrm{s} = 1.33\,\mathrm{mbar}\cdot 1\,\mathrm{s} \qquad \textit{(Eq. 3.15)}.$$

Sputter sources

Sputter sources were not used to deposit materials but to clean substrates by etching. They accelerate noble gas ions (Ar^+ in our case) with an electric field of some kV. They have been used to clean metallic substrates after degassing and before thin film deposition. Typical conditions were 5 kV and 2 µA for 5 minutes.

3.4 Ex-situ characterization techniques

3.4.1 AFM

The atomic force microscope (AFM), invented in 1986 by Binnig, Quate and Gerber [147], utilizes a sharp tip moving over the sample surface in a raster scan. The tip is on the end of a cantilever which bends in response to the force between the tip and the sample. The light from a laser is reflected by the cantilever onto a position-sensing photo-diode. As the cantilever flexes the bending can be measured. Since the cantilever obeys Hooke's law for small displacements, the interaction force between the tip and the sample can be found. The movement of the tip or sample is performed by an extremely precise positioning device of piezo-electric ceramics, capable of sub-angstrom resolution in x-, y- and z-directions. An electronic feedback controls the positioning piezo in z-direction, responding to any detected changes in force, and alters the tip-sample separation to restore the force to a pre-determined value. This mode of operation is known as constant force, and is used to reproduce the sample topography. If this constant force is in the repulsive region of the inter-molecular interaction the measurement is in contact mode.

3.4.2 TEM

The transmission electron microscope was first developed around 1930 after the effective role of wavelength on the theoretical resolution was noticed. The path of electron as charged particle can easily be controlled by a magnetic field. Also, it can be accelerated by electrical potential gradients. Faster electrons allow better resolution as according to the de Broglie relationship they have shorter wavelengths. The wavelength corresponding to 100 kV acceleration voltage is 0.0037 nm, much smaller as can be obtained by any other typical probing particle such X-rays or neutrons. Modern instruments can achieve lateral resolution better than 0.2 nm.

An electron beam is focused onto a thin sample, and magnetic lenses transform the image to a fluorescent screen, a film plate or a video camera. With samples of 200 nm thickness scattering from the interaction with matter are limited and beam coherence is maintained. In presence of crystalline phases besides the transmitted beam also a diffracted beam originates from the sample. Contrast images can be originated by transmission, showing inhomogeneities in thickness or composition (with light and heavy atoms unevenly distributed), or by diffraction. In vicinity of a lattice defect a diffraction inhomogeneity may occur, which corresponds to a local variation of the diffracted vs. transmitted intensity. In high-resolution mode at high magnification periodic fringes may be visible representing a direct resolution of Bragg diffraction planes. The observed contrast is then referred to as a phase contrast.

To avoid any interference with the sample holder an amorphous carbon substrate was deposited onto a gold grid. Also in this case TiS_2 was deposited over a metallic Ti layer. The sample was then transferred to the microscope without avoiding contact with air.